Journal of Inorganic and General Chemistry
ZAAC
Zeitschrift für anorganische und allgemeine Chemie
DOI: 10.1002/zaac.201900188
ARTICLE

Polymorphism of Ba_2SiP_4

Arthur Haffner,[a] Valentin Weippert,[a] and Dirk Johrendt*[a]

Dedicated to Professor Hans-Jörg Deiseroth on the Occasion of his 75th Birthday

Abstract. The three-dimensional SiP_4 network in the known phosphidosilicate Ba_2SiP_4-*tI*28 is analogous to β-Cristobalite if oxygen is formally replaced by P–P dimers. Here we report a second polymorph Ba_2SiP_4-*oP*56 [*Pnma*, a = 12.3710(4) Å, b = 14.6296(7) Å, c = 7.9783(3) Å; Z = 8] with chains of SiP_4 tetrahedra connected by P–P bonds, reminiscent to the elusive fibrous SiO_2. Ba_2SiP_4 is enantiotropic. The high temperature polymorph Ba_2SiP_4-*oP*56 transforms to the low-temperature phase Ba_2SiP_4-*tI*28 at 650 °C and reconstructs to the high-temperature modification at 1100 °C. DFT calculations predict an indirect optical bandgap of about 1.7 eV.

Introduction

Phosphidosilicates are known since the 1980s and attract anew considerable interest due to its broad structural variety involving compounds with versatile properties. The structures based on SiP_4 tetrahedra as anionic basic building unit are closely related to oxido- and nitridosilicates indicating a large structural variety. The nesosilicates Li_8SiP_4,[1] EA_4SiP_4 (*EA* = Ca, Sr, Ba)[2] or $Na_4EA_2SiP_4$ (*EA* = Ca, Sr, Eu)[3] are rare examples of isolated highly charged $[SiP_4]^{8-}$ anions. More common are SiP_4 anions with reduced charge density achieved by different condensation degrees leading to chains, layers, or three-dimensional network motifs. $A_{10}Si_2P_6$ (*A* = Li, Na)[4] exhibits edge-shared $[Si_2P_6]^{10-}$ entities whereas the charge density is decreased furthermore by edge condensation of these units to infinite $[SiP_2]^{2-}$ chains found in K_2SiP_2.[5] Interestingly, to date layered phosphidosilicates were only observed with supertetrahedral entities constituted of vertex sharing SiP_4 tetrahedra in $CaSiP_2$[6] and KSi_2P_3.[7] In contrast, the introduction of small and weak electronegative metals yields three-dimensional structures of vertex-shared tetrahedra[8] or supertetrahedra with sizes ranged from T2 to T5[9] and the feature of supertetrahedral fusion in Li_2SiP_2, $LiSi_2P_3$[10] and $Na_{23}Si_{9n+19}P_{12n+33}$ with n = 0–3.[11] To the best of our knowledge this uncommon condensation mode was sparely observed only in KSi_2P_3,[7] B_2S_3,[12] $Li_9B_{19}S_{33}$,[13] $M_{15}Tr_{22}As_{32}$ and $M_3Ga_6As_8$ (*M* = Sr, Eu; *Tr* = Ga, In)[14] and a few other mixed-metal T3 chalcogenides.[15]

The possibility of the formation of homonuclear phosphorus bonding distinguishes the family of phosphidosilicates from the oxido- and nitridosilicates. Isolated P–P bonding was described in $AlSiP_3$,[16] $Ca_3Si_8P_{14}$,[6] $Ba_2Si_3P_6$[17] and $Ba_4Si_3P_8$,[18] for example, whereas in $LaSi_2P_6$ up to four different polyphosphide anions $(P_n)^{-(n+2)}$ with n = 3–6 and in $Li_3Si_3P_7$[4a] polyphosphide chains exist. Tetragonal Ba_2SiP_4-*tI*28[19] is the first example where all SiP_4 tetrahedra are connected by P–P bonds. Currently the Ba-Si-P ternary system attracts attention regarding possible NLO and thermoelectric properties.[17] Therefore, we focused upon this compounds and found the high-temperature enantiotropic polymorph Ba_2SiP_4-*oP*56, in which all SiP_4 tetrahedra are linked by homonuclear phosphorus bonds, as well, being the second example for this structure motif.

Results and Discussion

Ba_2SiP_4-*oP*56 was synthesized by solid-state reactions of stoichiometric amounts of respective elements under inert conditions revealing air sensitive polycrystalline black powders. Single crystals suitable for single-crystal X-ray diffraction were selected under dried paraffin oil. The compound crystallizes in a primitive orthorhombic unit cell in space group

Table 1. Crystallographic data of Ba_2SiP_4-*oP*56.

	Ba_2SiP_4
space group	*Pnma* (no. 62)
a /Å	12.3710(4)
b /Å	14.6296(7)
c /Å	7.9783(3)
V_{cell} /Å^3	1443.93(10)
Z	8
ρ_{X-ray} /g·cm^{-3}	3.925
μ /mm^{-1}	11.773
Θ-range / °	2.785–30.527
Reflections measured	14530
Independent reflections	2286
Parameters	67
R_σ	0.0343
R_{int}	0.0596
R_1 [$F^2>2\sigma(F^2)$] / all	0.0281 / 0.0448
wR_2 [$F^2>2\sigma(F^2)$] / all	0.0470 / 0.0509
Goof	1.095
$\Delta\rho_{max/min}$ /e·Å^{-3}	1.536 / –1.293

* Prof. Dr. D. Johrendt
E-Mail: johrendt@lmu.de
[a] Department of Chemistry
Ludwig-Maximilians-University of Munich
Butenandtstrasse 5–13 (D)
81377 Munich, Germany

Table 2. Fractional coordinates, Wyckoff positions, and equivalent displacement parameters of Ba_2SiP_4-*oP*56.

Atom	Wyckoff position	*x*	*y*	*z*	U_{eq} /Å^2
Ba1	8*d*	0.34858 (2)	0.51347(2)	0.38205(4)	0.01148(7)
Ba2	4*c*	0.26291(4)	1/4	0.22464(6)	0.01343(9)
Ba3	4*c*	0.43469(4)	1/4	0.72852(6)	0.0173(1)
Si1	8*d*	0.04023(11)	0.11551(10)	0.38639(17)	0.0094(2)
P1	8*d*	0.01981(11)	0.17373(9)	0.12824(17)	0.0116(2)
P2	8*d*	0.09964(10)	0.51730(9)	0.28240(15)	0.0108(2)
P3	8*d*	0.16274(11)	0.17243(10)	0.57072(17)	0.0136(3)
P4	8*d*	0.37387(10)	0.10051(9)	0.00761(16)	0.0104(2)

Pnma with lattice parameters a = 12.3710(4) Å, b = 14.6296(7) Å, and c = 7.9783(3) Å. The structure was solved and refined using the SHELX[20] package. Crystallographic data of Ba_2SiP_4-*oP*56 are given in Table 1, fractional coordinates and equivalent displacement parameters in Table 2. Based on this data the powder pattern of a polycrystalline sample was indexed and refined yielding in about 94 wt-% of the targeted phase with small impurities of the low-temperature polymorph Ba_2SiP_4-*tI*28,[19] Ba_3P_4[21] and a minor unidentified phase (Figure 1).

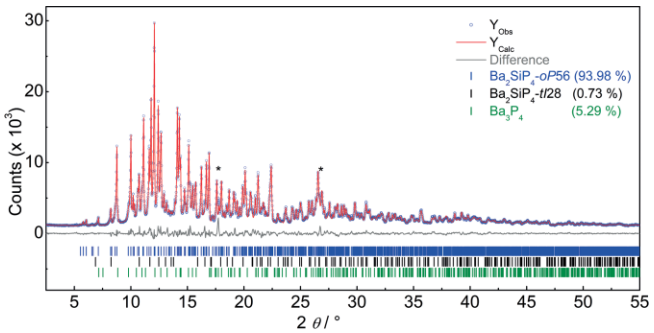

Figure 1. X-ray powder pattern of the Ba_2SiP_4-*oP*56 sample (blue circles) with Rietveld fit (red line) and difference (grey line). Small amounts of Ba_2SiP_4-*tI*28 and Ba_3P_4, beside an unknown impurity, marked with asterisks, were detected.

The polycrystalline sample was further investigated by solid-state MAS-NMR and EDX, confirming the elemental composition. Figure 2 shows the ^{31}P spectrum with four distinct resonance frequencies at δ (P) = –67.98, –118.33, –125.92, –157.23 ppm, each with the same intensity indicating four magnetically inequivalent phosphorus atoms with the same multiplicity, which is in accordance with the single crystal structure. The examined sample contains 5 wt-% Ba_3P_4 in Sr_3As_4 type structure with two crystallographically different phosphorus atoms.[21] This impurity is visible in the ^{31}P NMR spectrum with two additional resonance frequencies at δ (P) = –48.35 and –84.40 ppm (see Figure 2, red crosses).

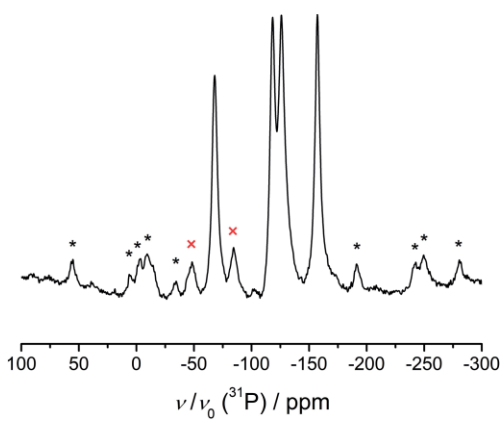

Figure 2. ^{31}P solid-state MAS-NMR spectrum of Ba_2SiP_4-*oP*56. Rotation side bands are marked with asterisks and resonance frequencies of the Ba_3P_4 impurity with red crosses.

Ba_2SiP_4-*oP*56 crystallizes in a new structure type with a unique structural motif composed of SiP_4 tetrahedra. As in Ba_2SiP_4-*tI*28, P–P bonds [$\varnothing d$(P–P) = 2.23 Å] link all SiP_4 tetrahedra, but here the connectivity generates chains along the *b* axis (Figure 3). The chains form a distorted hexagonal rod packing, similar to the chains of edge-sharing $SiS_{4/2}$ tetrahedra in SiS_2.[22] As we mentioned earlier, the three-dimensional network in Ba_2SiP_4-*tI*28 is analogous to β-Cristobalite, if one replaces the oxygen atoms in SiO_2 by P_2 dimers. In this sense, the new chain structure of Ba_2SiP_4-*oP*56 would be the analogue of the fibrous SiO_2, which is still elusive.[23]

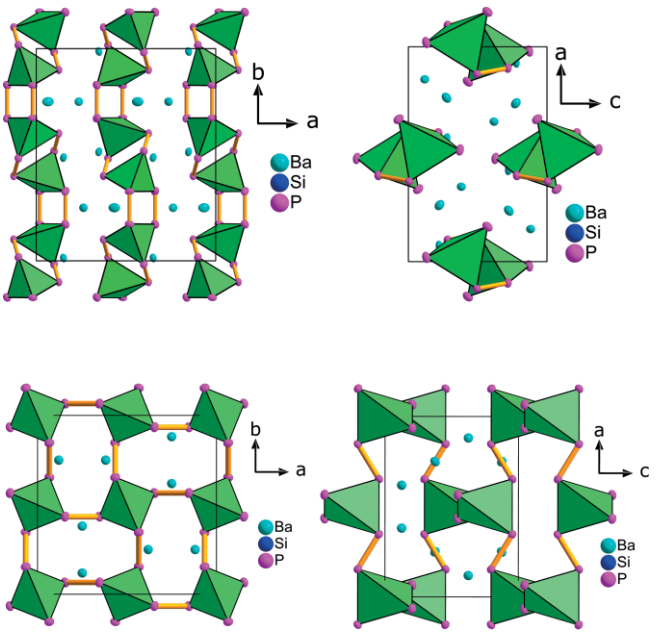

Figure 3. Crystal structure of Ba_2SiP_4-*oP*56 with view along [001] (top, left) and along [010] (top, right) and Ba_2SiP_4-*tI*28 with respective viewing directions (bottom). Ellipsoids are drawn with 90% probability.

The Ba^{2+} cations are located between the anionic chains in strongly distorted polyhedra, which are gyro-elongated square pyramids (Ba1) with one, cubes (Ba2) with three or elongated square bipyramids (Ba3) with five homonuclear phosphorus bonds as depicted in Figure 4.

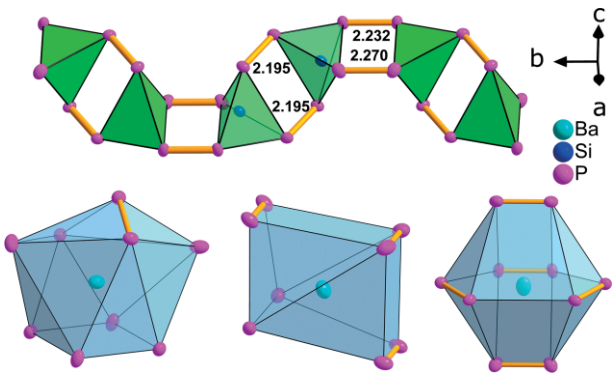

Figure 4. $^{1}_{\infty}[SiP_4]^{4-}$ chain motif of *pseudo* edge-condensed SiP_4 tetrahedra (top) and Ba coordinations containing homonuclear phosphorus bonds of Ba1 (left), Ba2 (middle) and Ba3 (right). All BaP_x polyhedra are strongly distorted.

Ba_2SiP_4-*oP*56 does not form if the solid state reactions are carried out at increased temperatures of 1100 °C with the slow cooling rates used for Ba_2SiP_4-*tI*28.[19] A nearly phase-pure sample could only be obtained by faster cooling rates from –10 K·h^{-1} to –50 K·h^{-1}. We examined the phase transition of Ba_2SiP_4-*oP*56 to Ba_2SiP_4-*tI*28 by high-temperature powder diffraction yielding no transition until about 600 °C, before a mixture of both modifications occurs near 650 °C. At 700 °C, Ba_2SiP_4-*oP*56 is almost completely transformed to Ba_2SiP_4-*tI*28, which persists upon cooling to room temperature (Figure 5). The additional reflection at about $2\Theta = 12°$ above 850 °C is probably caused by crystallizing of the silica capillary. On the other hand Ba_2SiP_4-*oP*56 can also be obtained from Ba_2SiP_4-*tI*28 if the same heating protocol is applied with faster cooling, thus Ba_2SiP_4 is enantiotropic with reconstructive phase transitions.

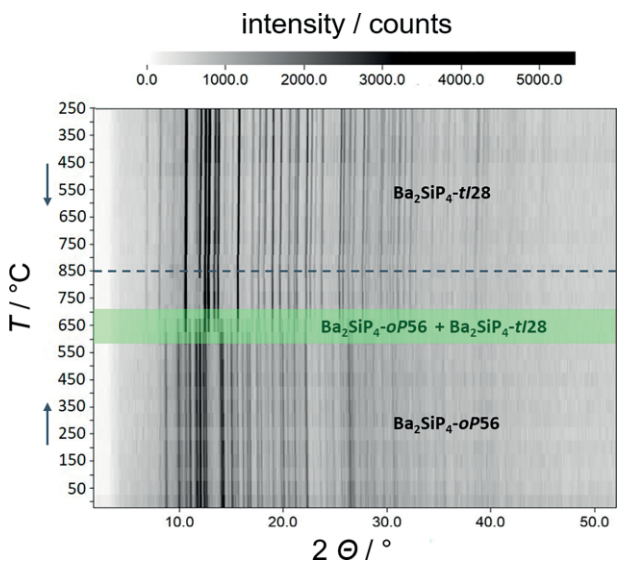

Figure 5. High-temperature powder diffraction pattern of Ba_2SiP_4. The sample was heated to 850 °C (marked with dashed line) and then cooled to 250 °C. Phase transition occurs between 600 and 700 °C (highlighted in green).

For the estimation of the electronic properties of Ba_2SiP_4-*oP*56 DFT calculations were performed. Figure 6 shows the electronic band structure and the atom-resolved density-of-states for Ba_2SiP_4-*oP*56. The valence band is dominated by the P-3p states with some contributions of Si-3p and Ba-5d. The energy gap is 1.11 eV using the PBE and increases to 1.65 eV with the mBJ functional. The valence band maximum is located at the Γ-point in the Brillouin zone and the conduction band minimum occurs at *T*, which means that the calculation predicts an indirect bandgap.

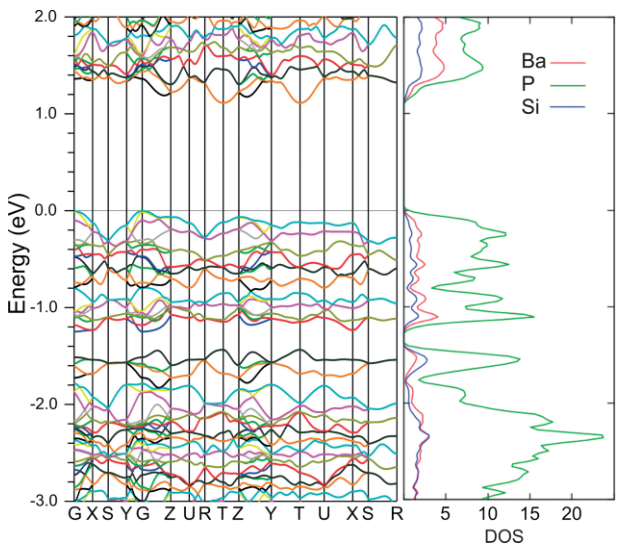

Figure 6. Electronic band structure (left) and atom-resolved DOS (right) for Ba_2SiP_4-*oP*56. The energy zero is taken at the Fermi level.

Conclusions

Ba_2SiP_4-*oP*56 crystallizes in a new structure type constituting the second example of a phosphidosilicate with all phosphorus atoms connected by P–P bonds. The crystal structure comprises SiP_4 tetrahedra bridged via P–P bonds, leading to $^{1}_{\infty}[SiP_4]^{4-}$ chains. While the network of tetragonal polymorph Ba_2SiP_4-*tI*28 is analogous to the β-Cristobalite type if one replaces oxygen by P_2 dimers, the chains in the new compound Ba_2SiP_4-*oP*56 are analogous to SiS_2, and reminiscent to the elusive fibrous SiO_2. A phase transition from Ba_2SiP_4-*oP*56 to Ba_2SiP_4-*tI*28 occurs at around 650 °C whereas we expect the re-transition well beyond 1000 °C, which we were not able to determine. Solid-state MAS-NMR data and its EDX fully confirm the structure. DFT calculations reveal an indirect bandgap of around 1.7 eV in agreement with the black color of the compound.

Experimental Section

Synthesis: Ba_2SiP_4-*oP*56 was obtained by two different routes. Either a stoichiometric mixture of respective elements (Ba, 99.99 %, Sigma

Aldrich; Si, 99.8 %, SMART ELEMENTS; P_{red}, > 99 %, CHEMPUR) or a phase-pure sample of Ba_2SiP_4-*tI*28 was heated to 1100 °C with a 50 K·h^{-1} rate for the elemental or with a 200 K·h^{-1} rate for the Ba_2SiP_4-*tI*28 route in alumina crucibles welded in argon filled silica ampoules. This temperature was held for 40 h before it was decreased to 450 °C with a relatively fast cooling rate of –50 K·h^{-1}. After cooling to room temperature the targeted product was received as polycrystalline and air sensitive black powder.

Single-Crystal X-ray Diffraction: Due to air sensitivity single crystals of sufficient quality were selected under dried paraffin oil and transferred in oil filled and fused Hilgenberg glass capillaries with 0.2 mm in diameter. Diffraction data were collected by a Bruker D8 Venture diffractometer with a rotating anode, Göbel mirror optics and a Photon II detector. Reflection indexing, data reduction and absorption correction were processed by the Bruker software APEX3.[24] Based on systematically absent reflections the space group of Ba_2SiP_4-*oP*56 was identified with XPREP.[25] Final solution and refinement of the crystal structure were performed with direct methods implemented in the SHELX software package.[20] For visualization of the crystal structure Diamond[26] software was chosen.

Powder X-ray Diffraction: A ground sample was loaded and sealed in a glass capillary with 0.2 mm in diameter (Hilgenberg GmbH) to avoid hydrolysis. Diffraction patterns were recorded on a Stadi-P powder diffractometer in Debye–Scherrer setup (STOE & Cie GmbH) equipped with a Ge monochromator, a Mythen 1 K detector (Dectris) and Mo-$K_{\alpha1}$ radiation. Diffractograms were indexed and refined using the single-crystal structure model and the Rietveld method implemented in the TOPAS[27] software.

Temperature-Dependent Powder X-ray Diffraction: For the investigation of the phase transition a ground sample was loaded into a silica capillary with 0.5 mm in diameter (Hilgenberg GmbH) and sealed with grease for pressure compensation while heating. Data were collected under argon atmosphere also on a Stadi-P diffractometer (STOE & Cie) with a Ge monochromator, an IP-PSD detector, a resistance graphite furnance and Mo-$K_{\alpha1}$ radiation. The sample was heated to 850 °C and cooled to room temperature in steps of 50 °C with a 5 K·min^{-1} rate. At each step, the temperature was kept constant and a diffraction pattern was collected. We were not able to measure the retransition from Ba_2SiP_4-*tI*28 to Ba_2SiP_4-*oP*56 beyond 1000 °C because of the limited chemical stability of the silica capillaries.

Solid-State MAS-NMR Spectroscopy: For the nuclear magnetic resonance spectrum of the ^{31}P nuclei a polycrystalline sample of Ba_2SiP_4-*oP*56 was loaded into a commercial zirconia rotor with 2.5 mm in diameter and placed into a Bruker Avance III 500 spectrometer device with a magnetic field of 11.74 T. The sample was rotated under MAS conditions with a frequency of 25 kHz and a Larmor frequency of ν_0 (^{31}P) = 202.5 MHz.

EDX Analysis: For elemental analysis, a sample was prepared under argon atmosphere onto adhesive and conductive carbon pads, which were inserted into an EVO-MA 10 (Zeiss) scanning electron microscope quickly. An electron beam was generated by a field emission gun. Characteristic X-ray radiation was detected by X-Flash 410-M (Bruker) and processed with QUANTAX 200 software package. Oxygen signals were not taken into account due to partial hydrolysis while inserting the sample.

Electronic Structure Calculations: The electronic band structure was calculated using the full-potential-linear-augmented plane-wave (FLAPW) method with the WIEN2k package.[28] Exchange and correlation were treated with the PBE[29] or mBJ[30] functionals. The experimental lattice parameters and atom positions were used for the band and DOS calculations shown in Figure 6. Tentatively optimizations of the atom positions showed no significant changes.

Acknowledgements

The authors thank *C. Minke* for assistance with the MAS-NMR measurements. Financial support by the Deutsche Forschungsgemeinschaft (DFG) is gratefully acknowledged.

Keywords: Phosphidosilicates; Enantiotropic phase transition; Pseudo edges; Barium; Semiconductors

References

[1] L. Toffoletti, H. Kirchhain, J. Landesfeind, W. Klein, L. van Wüllen, H. A. Gasteiger, T. F. Fässler, *Chem. Eur. J.* **2016**, *22*, 17635–17645.
[2] B. Eisenmann, H. Jordan, H. Schäfer, *Mater. Res. Bull.* **1982**, *17*, 95–99.
[3] J. Nuss, H. Kalpen, W. Hönle, M. Hartweg, H. G. von Schnering, *Z. Anorg. Allg. Chem.* **1997**, *623*, 205–211.
[4] a) H. Eickhoff, L. Toffoletti, W. Klein, G. Raudaschl-Sieber, T. F. Fässler, *Inorg. Chem.* **2017**, *56*, 6688–6694; b) B. Eisenmann, M. Somer, *Z. Naturforsch. B* **1985**, *40*, 886–890.
[5] B. Eisenmann, M. Somer, *Z. Naturforsch. B* **1984**, *39*, 736–738.
[6] X. Zhang, T. Yu, C. Li, S. Wang, X. Tao, *Z. Anorg. Allg. Chem.* **2015**, *641*, 1545–1549.
[7] K. Feng, L. Kang, W. Yin, W. Hao, Z. Lin, J. Yao, Y. Wu, *J. Solid State Chem.* **2013**, *205*, 129–133.
[8] a) A. J. Springthorpe, J. G. Harrison, *Nature* **1969**, *222*, 977; b) A. A. Vaipolin, E. O. Osmanov, D. N. Tretyakov, *Inorg. Mater.* **1967**, *3*, 231–236.
[9] H. Li, J. Kim, T. L. Groy, M. O'Keeffe, O. M. Yaghi, *J. Am. Chem. Soc.* **2001**, *123*, 4867–4868.
[10] A. Haffner, T. Bräuniger, D. Johrendt, *Angew. Chem. Int. Ed.* **2016**, *55*, 13585–13588.
[11] A. Haffner, A.-K. Hatz, I. Moudrakovski, B. V. Lotsch, D. Johrendt, *Angew. Chem. Int. Ed.* **2018**, *57*, 6155–6160.
[12] T. Sasaki, H. Takizawa, K. Uheda, T. Yamashita, T. Endo, *J. Solid State Chem.* **2002**, *166*, 164–170.
[13] F. Hiltmann, P. zum Hebel, A. Hammerschmidt, B. Krebs, *Z. Anorg. Allg. Chem.* **1993**, *619*, 293–302.
[14] V. Weippert, A. Haffner, A. Stamatopoulos, D. Johrendt, *J. Am. Chem. Soc.* **2019**, *141*, 11245–11252.
[15] a) H. Lin, J.-N. Shen, L. Chen, L.-M. Wu, *Inorg. Chem.* **2013**, *52*, 10726–10728; b) W. Khan, S. Goumri-Said, *RSC Adv.* **2015**, *5*, 9455–9461; c) H. Li, C. D. Malliakas, Z. Liu, J. A. Peters, H. Jin, C. D. Morris, L. Zhao, B. W. Wessels, A. J. Freeman, M. G. Kanatzidis, *Chem. Mater.* **2012**, *24*, 4434–4441; d) J. H. Liao, M. G. Kanatzidis, *Chem. Mater.* **1993**, *5*, 1561–1569; e) H.-W. Ma, G.-C. Guo, M.-S. Wang, G.-W. Zhou, S.-H. Lin, Z.-C. Dong, J.-S. Huang, *Inorg. Chem.* **2003**, *42*, 1366–1370.
[16] H. G. von Schnering, G. Menge, *J. Solid State Chem.* **1979**, *28*, 13–19.
[17] J. Mark, J. Wang, K. Wu, J. G. Lo, S. Lee, K. Kovnir, *J. Am. Chem. Soc.* **2019**, *141*, 11976–11983.
[18] J. Mark, J.-A. Dolyniuk, N. Tran, K. Kovnir, *Z. Anorg. Allg. Chem.* **2019**, *645*, 242–247.
[19] A. Haffner, D. Johrendt, *Z. Anorg. Allg. Chem.* **2017**, *643*, 1717–1720.
[20] G. M. Sheldrick, *Acta Crystallogr., Sect. A* **2008**, *64*, 112–122.
[21] H.-G. von Schnering, M. Wittmann, D. Sommer, *Z. Anorg. Allg. Chem.* **1984**, *510*, 61–71.

[22] W. Büssem, H. Fischer, E. Gruner, *Naturwissenschaften* **1935**, *23*, 740.
[23] A. Weiss, A. Weiss, *Z. Anorg. Allg. Chem.* **1954**, *276*, 95–112.
[24] Bruker AXS Inc., APEX3 Version 2016.5–0, Madison, Wisconsin, **2016**.
[25] Bruker AXS Inc., XPREP Version 2008/2, Karlsruhe, Germany, **2008**.
[26] K. Brandenburg, Diamond Version 3.2k, Crystal Impact GbR, Bonn, Germany, **2014**.
[27] A. Coelho, Topas Academic Version 4.1, Coelho Software, Brisbane, Australia, **2007**.
[28] P. Blaha, K. Schwarz, G. K. H. Madsen, D. Kvasnicka, J. Luitz, Wien2k, An Augmented Plane Wave and Local Orbital Program for Calculating Crystal Properties, TU Wien, Vienna, Austria, ISBN3–9501031–1-2, 2006.
[29] J. P. Perdew, S. Burke, M. Ernzerhof, *Phys. Rev. Lett.* **1996**, *77*, 3865–3868.
[30] F. Tran, P. Blaha, *Phys. Rev. Lett.* **2009**, *102*, 226401.

Received: August 9, 2019
Published Online: November 8, 2019

